Supplementary material for LHCb-PAPER-2018-009

This appendix contains supplementary material that will posted on the public CDS record but will not appear in the paper.

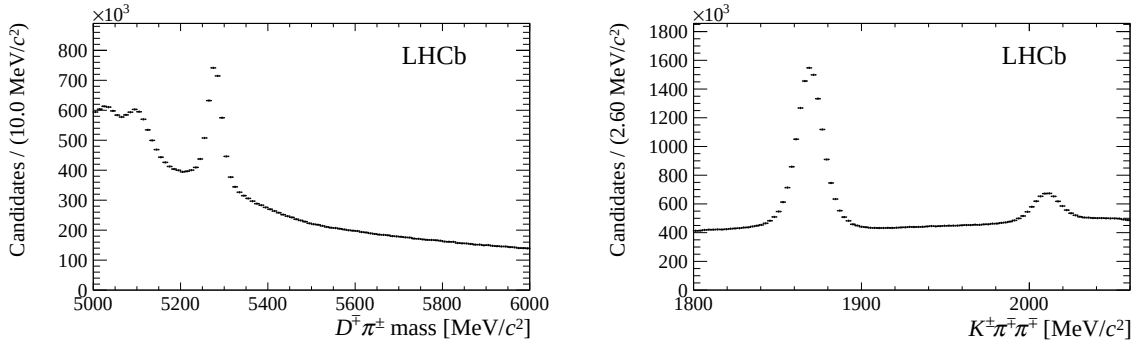

Figure 1: (Left) $D\pi$ and (right) $K\pi\pi$ invariant mass distributions of the reconstructed candidates after the online event selection.

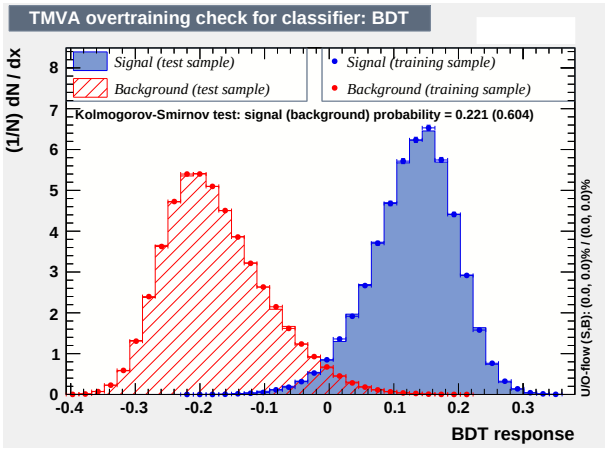

Figure 2: Output of the BDT classifier for the (blue) signal and (red) background samples. The points show the distributions of the training samples, the shaded areas the distributions of the test samples.

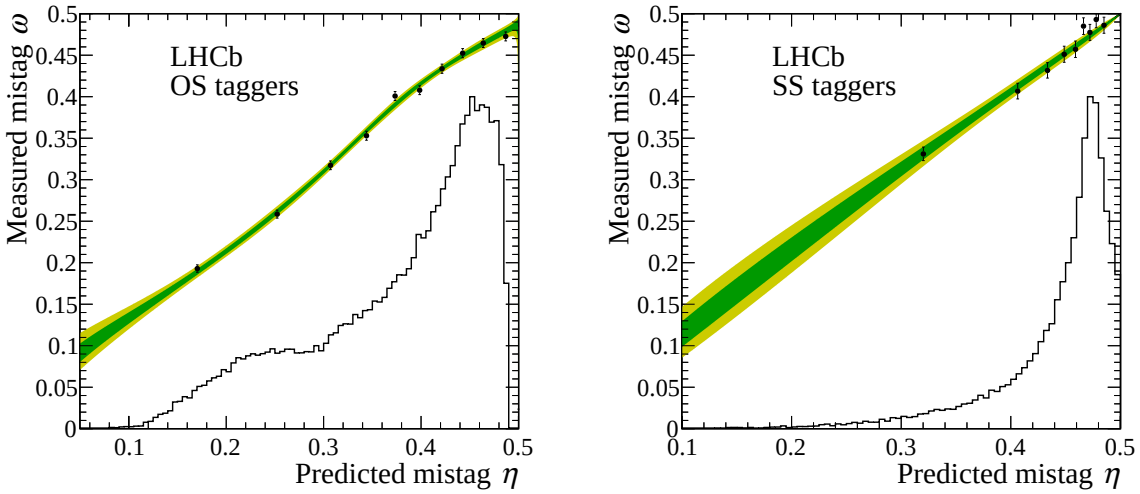

Figure 3: Measured mistag fraction ω versus predicted mistag probability η of the combination of (left) OS and (right) SS taggers as determined in control data. The black histograms are the distributions of the mistag probabilities in arbitrary units. The shaded areas correspond to the 68% and 95% confidence level regions of the calibration functions and do not include systematic uncertainties on the parameters. The calibration functions and the distributions of mistag probabilities are shown summing over candidates tagged either as B^0 or $\overline{B}^0$.

Table 1: Correlation matrix of S_f, $S_{\bar{f}}$, $A_{\rm P}$, $A_{\rm D}$, Δm and Γ parameters obtained from the fit to the $B^0 \to D^{\mp}\pi^{\pm}$ decay time.

	S_f	$S_{\bar{f}}$	$A_{\rm P}$	$A_{\rm D}$	Δm	Γ
S_f	1	0.44	−0.11	−0.05	−0.34	0.00
$S_{\bar{f}}$		1	−0.10	−0.07	0.29	0.00
$A_{\rm P}$			1	0.58	0.00	0.00
$A_{\rm D}$				1	0.00	0.00
Δm					1	0.00
Γ						1

Table 2: Matrix of statistical correlations among S_f, $S_{\bar{f}}$, $A_{\rm P}$ and $A_{\rm D}$ parameters obtained from the fit to the $B^0 \to D^{\mp}\pi^{\pm}$ decay time with Δm and Γ fixed to the central values used in the Gaussian constraints.

	S_f	$S_{\bar{f}}$	$A_{\rm P}$	$A_{\rm D}$
S_f	1	0.60	−0.12	−0.06
$S_{\bar{f}}$		1	−0.11	−0.07
$A_{\rm P}$			1	0.58
$A_{\rm D}$				1

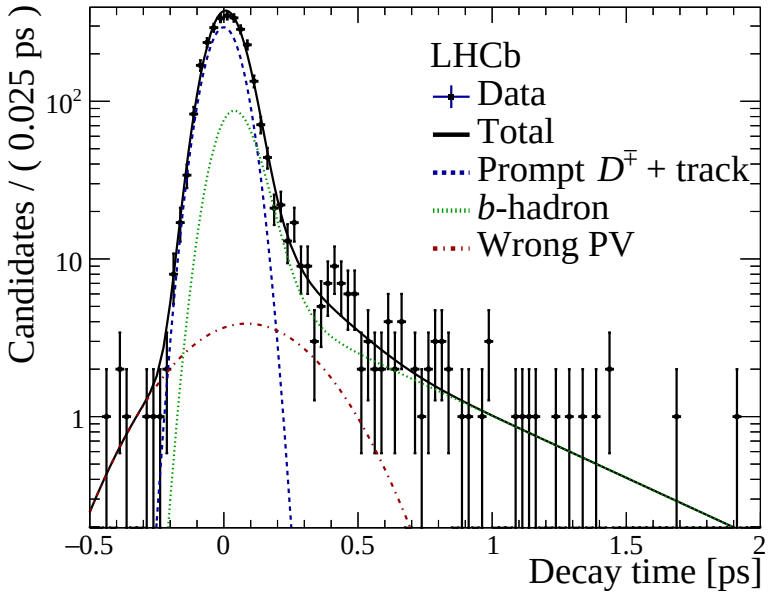

Figure 4: Decay-time distribution for one illustrative bin in per-candidate decay-time error for *fake* B^0 candidates. As the decay-time resolution is dependent upon the transverse momentum of the companion track, the *fake* B^0 candidates are weighted in transverse momentum to match the signal $B^0 \to D^{\mp}\pi^{\pm}$ candidates. A fit is overlaid in black. The wrong-PV component is shown in red, dot-dashed. The component due to b-hadron decays is shown in green, dotted, and the prompt component is shown in blue, dashed.

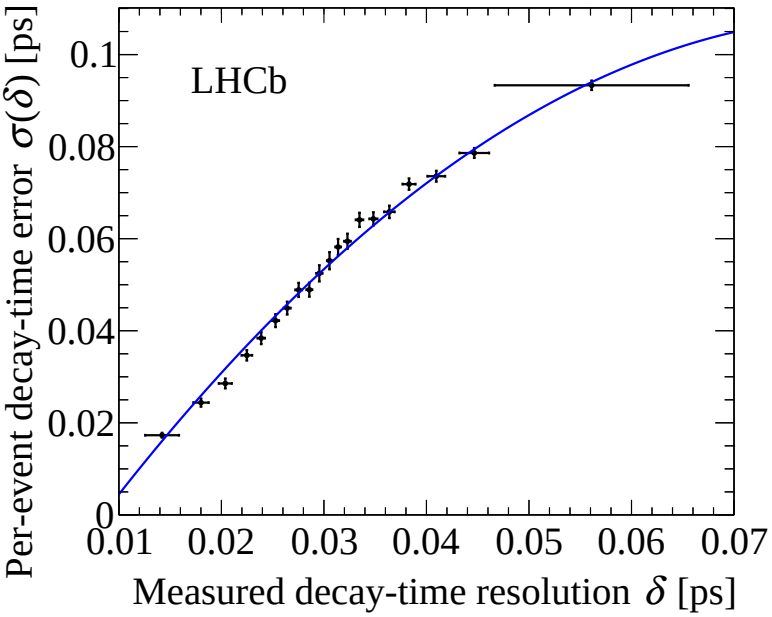

Figure 5: Measured resolution versus average per-candidate decay-time error determined from fits to the decay time in bins of decay time error. The horizontal-axis uncertainties are the standard deviation of the average per-candidate decay time error in each bin. A χ^2 fit of the form $\langle\sigma\rangle_i = \langle\sigma\rangle + p_1\left(\langle\delta\rangle_i - \langle\delta\rangle\right) + p_2\left(\langle\delta\rangle_i - \langle\delta\rangle\right)^2$ is overlaid.

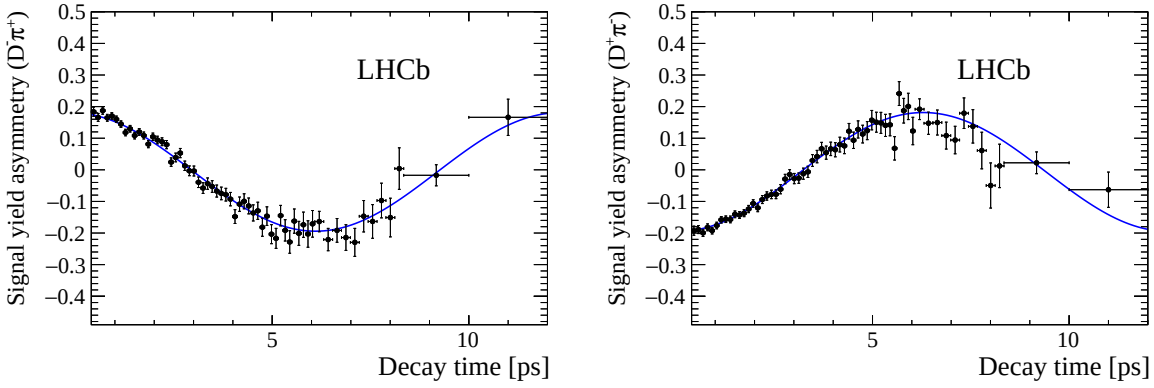

Figure 6: Decay-time-dependent signal-yield asymmetry for the (left) $D^-\pi^+$ and the (right) $D^+\pi^-$ final states. The signal-yield asymmetry is defined as the difference between candidates tagged as B^0 and $\overline{B}^0$ divided by their sum. The solid curve is the projection of the signal PDF.

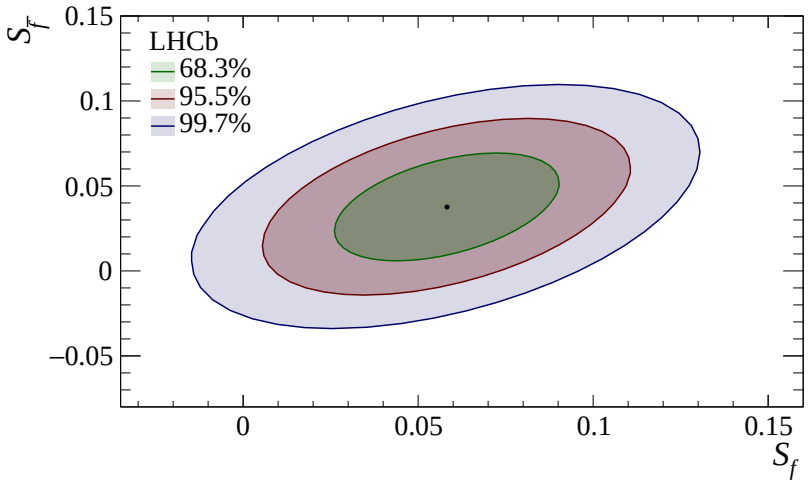

Figure 7: Contour plot for (S_f, $S_{\bar{f}}$) showing the one, two and three sigma contours. The uncertainties include the full statistical uncertainty and the systematic uncertainty due to Gaussian constraints on the mixing frequency Δm and the B^0 decay width Γ.

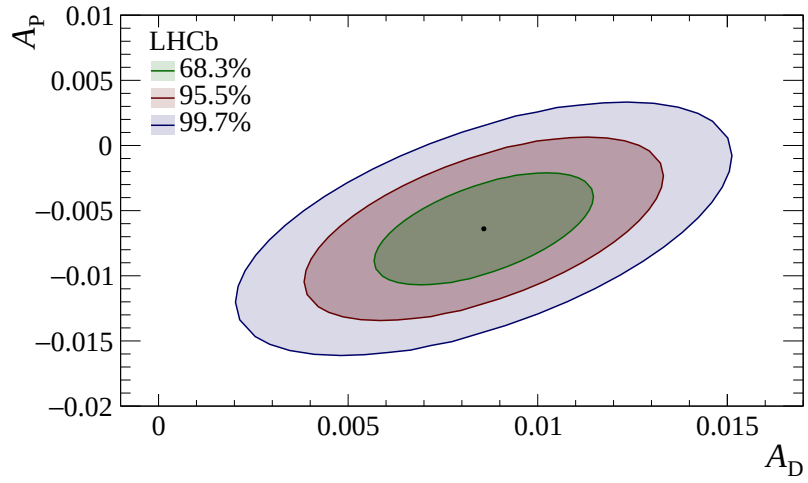

Figure 8: Contour plot for (A_P, A_D) showing the one, two and three sigma contours. The uncertainties include the full statistical uncertainty and the systematic uncertainty due to Gaussian constraints on the mixing frequency Δm and the B^0 decay width Γ.

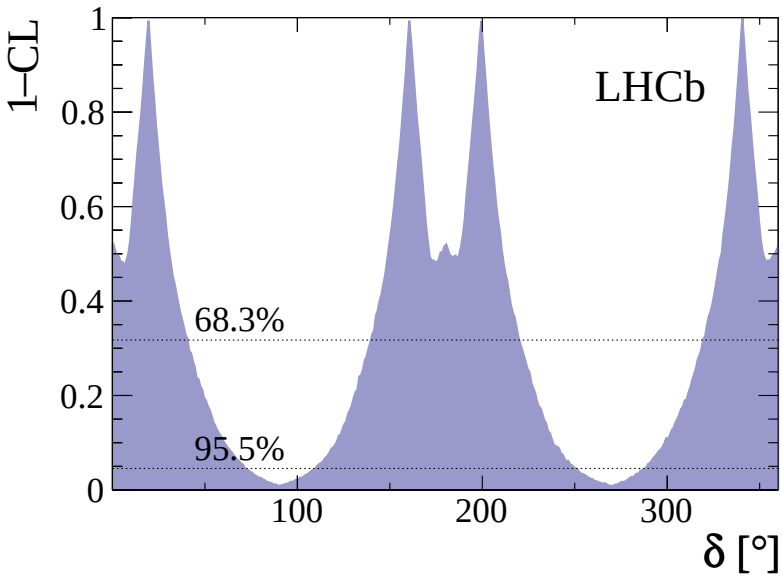

Figure 9: 1–CL as a function of δ obtained using the measured values of S_f and $S_{\bar{f}}$.

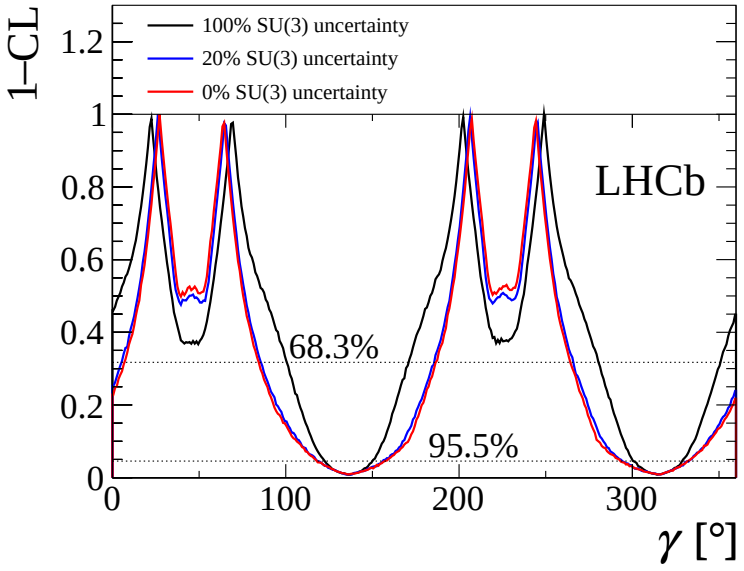

Figure 10: 1–CL as a function of γ for assumptions of 0%, 20% and 100% for the non-factorisable SU(3) breaking uncertainty on the parameter $r_{D\pi}$.

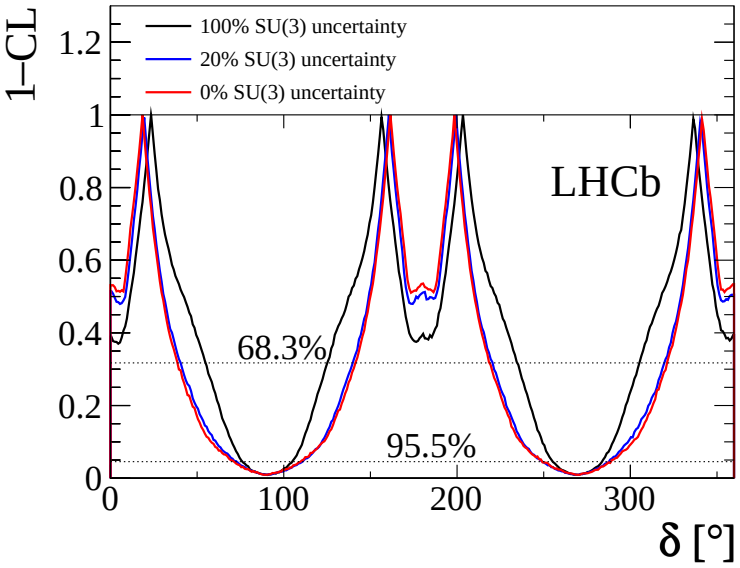

Figure 11: 1–CL as a function of δ for assumptions of 0%, 20% and 100% for the non-factorisable SU(3) breaking uncertainty on the parameter $r_{D\pi}$.

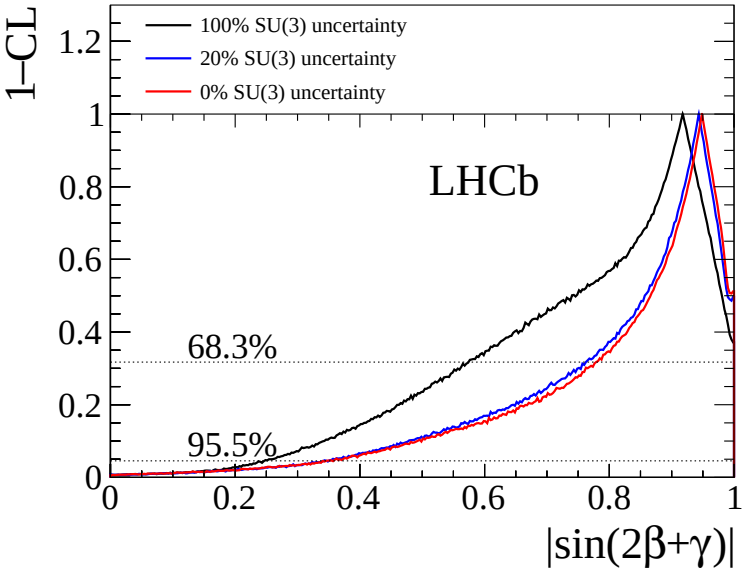

Figure 12: 1–CL as a function of $|\sin(2\beta+\gamma)|$ for assumptions of 0%, 20% and 100% for the non-factorisable SU(3) breaking uncertainty on the parameter $r_{D\pi}$.